ChemPubSoc Europe

DOI: 10.1002/chem.201600125

CHEMISTRY A European Journal Full Paper

Nanotechnology

A Red to Near-IR Fluorogen: Aggregation-Induced Emission, Large Stokes Shift, High Solid Efficiency and Application in Cell-Imaging

Yi Jia Wang,[a] Yang Shi,[a] Zhaoyang Wang,[a] Zhenfeng Zhu,[b] Xinyuan Zhao,[c] Han Nie,[d] Jun Qian,[b] Anjun Qin,[d] Jing Zhi Sun,*[a] and Ben Zhong Tang*[a, d, e]

Abstract: A tetraphenylethene (TPE) derivative modified with the strong electron acceptor 2-dicyano-methylene-3-cyano-4,5,5-trimethyl-2,5-dihydrofuran (TCF) was obtained in high yield by a simple two-step reaction. The resultant TPE-TCF showed evident aggregation-induced emission (AIE) features and pronounced solvatochromic behavior. Changing the solvent from apolar cyclohexane to highly polar acetonitrile, the emission peak shifted from 560 to 680 nm (120 nm redshift). In an acetonitrile solution and in the solid powder, the Stokes shifts are as large as 230 and 190 nm, respectively. The solid film emits red to near-IR (red-NIR) fluorescence with an emission peak at 670 nm and a quantum efficiency of 24.8%. Taking the advantages of red-NIR emission and high efficiency, nanoparticles (NPs) of TPE-TCF were fabricated by using tat-modified 1,2-distearoylsn-glycero-3-phosphor-ethanol-amine-*N*-[methoxy-(polyethyl-eneglycol)-2000] as the encapsulation matrix. The obtained NPs showed perfect membrane penetrability and high fluorescent imaging quality of cell cytoplasm. Upon co-incubation with 4,6-diamidino-2-phenylindole (DAPI) in the presence of tritons, the capsulated TPE-TCF nanoparticles could enter into the nucleus and displayed similar staining properties to those of DAPI.

Introduction

The development of fluorogens with red and/or near-IR (NIR) emission is nowadays one of the hottest topics of investigation in the field of bio/chemosensors and bioimaging.[1] Due to their long emission wavelengths and large Stokes shifts, these kinds of fluorogens allow the excitation and emission wavelengths to penetrate deeper into tissues, cause less damage to living cells than UV and visible wavelengths, and do not suffer from the autofluorescence of biomolecules in the short wavelength region.[2] Up to now, only a few such kinds of fluorogens, including boron-dipyrromethene (BODIPY),[3] rhodamine,[4] and squaraine[5] have been developed for biological applications. However, the development of efficient luminescent materials with red to NIR emission and large Stokes shifts is still challenging because most dyes are highly emissive in dilute solution but become weakly luminescent or even nonemissive in the condensed phase; this can be attributed to the formation of detrimental excimers and exciplexes. This so-called aggregation-caused quenching (ACQ) problem must be overcome because in some applications, it is necessary to use fluorescent dyes in high concentration or in the solid state.

Recently, new types of fluorogens showing the aggregation-induced emission (AIE) effect, which is the exact opposite of the ACQ effect, have received much research attention because of their unique optical properties and extensive applications.[6] Since the first AIE-active dye was observed in 2001,[7] more and more molecules with AIE properties have been designed and prepared. Among them, the derivatives with red emission have been successfully applied in the fields of chemo- and biosensors and cell imaging.[8] For example, by modifying the tetraphenylethene (TPE) core, one of the typical AIE-gens, with perylene bisimide[8a] and diphenylaminofumaronitrile groups,[8b] the obtained TPE derivatives were tested in tumor targeting and noninvasive long-term cell-imaging studies.

[a] *Y. J. Wang, Y. Shi, Z. Wang, Prof. J. Z. Sun, Prof. B. Z. Tang*
MoE Key Laboratory of Macromolecule Synthesis
and Functionalization Department of Polymer Science and Engineering
Zhejiang University, Hangzhou 310027 (China)
E-mail: sunjz@zju.edu.cn

[b] *Z. Zhu, Prof. J. Qian*
State Key Laboratory of Modern Optical Instrumentation
Centre for Optical and Electromagnetic Research
Zhejiang Provincial Key Laboratory for Sensing Technologies
JORCEP (Sino-Swedish Joint Research Centre of Photonics)
Zhejiang University, Hangzhou 310058 (China)

[c] *X. Zhao*
Institute of Environmental Health, Zhejiang University
Hangzhou 310058 (China)

[d] *H. Nie, Prof. A. Qin, Prof. B. Z. Tang*
Guangdong Innovative Research Team
State Key Laboratory of Luminescent Materials and Devices
South China University of Technology, Guangzhou 510640 (China)

[e] *Prof. B. Z. Tang*
Department of Chemistry, Institute for Advanced Study
State Key Laboratory of Molecular NeuroScience
and Division of Biomedical Engineering Institution
The Hong Kong University of Science and Technology
Clear Water Bay, Kowloon, Hong Kong (China)

Supporting information for this article can be found under http://dx.doi.org/10.1002/chem.201600125.

It is necessary for more AIE-active molecules with long emission wavelengths to be developed to meet application needs, not only for bioimaging and highly sensitive chemosensors, but also for the fabrication of full-color organic light-emitting diodes. Unfortunately, reports of such AIE molecules, especially those containing TPE moieties, displaying both AIE and large Stokes shift are still quite limited,[8,9] mainly due to the difficulty in their design and synthesis.

Results and Discussion

The synthetic route to the TPE-TCF conjugate is shown in Scheme 1. The detailed synthetic procedures and data of the structure characterization are described in the Experimental Section and Supporting Information (Scheme S1). The precursor, the aldehyde-functionalized TPE derivative (TPE-CHO), was prepared according to our previously published papers,[10] and TCF was easily obtained by a simple route (Scheme 1 and Scheme S1 in the Supporting Information). The target compound TPE-TCF was derived from a condensation reaction between the aldehyde group of TPE-CHO and the activated methyl of TCF, which proceeded smoothly and efficiently under mild conditions. The synthetic route to TPE-TCF is short and it contains only two facile steps. As a result, the overall yield of TPE-TCF was up to 72%, which is much higher than other reported red-emissive AIE fluorogens, such as TPE-modified perylenebisimide,[8a,11a] diphenylaminofumaronitrile,[11b] and BODIPY units.[9] The structural characterization data of the product by spectroscopic methods are given in the Experimental Section. The purity of the resultant products and intermediates has been confirmed by elemental analysis, ^{1}H NMR, ^{13}C NMR, and high-resolution mass (MALDI-TOF) spectroscopic techniques (see Figures S1–S3, Supporting Information).

With the aim of obtaining the expected fluorogens, a novel TPE derivative TPE-TCF has been designed and synthesized (see Scheme 1). Our strategy is based on the following design principles: Firstly, TPE is a typical AIE-gen that is widely used in designing AIE derivatives.[11] It was therefore highly likely to provide TPE-TCF with AIE properties. Secondly, the red-NIR emissive fluorogens should have a large conjugated system. The modifier of (2-(3-cyano-4,5,5-trimethylfuran-2(5*H*)-ylidene)-malononitrile) (TCF) is a fully conjugated system and linking it to the TPE core with a C=C double bond will extend the conjugation and lead to a redshifted emission. Thirdly, the TPE unit is an electron donor (D) and the TCF group with three cyano groups is a strong electron acceptor (A) thereby it can further redshift the emission spectrum by D–A interaction. Such D–A fluorophores often show the photophysical phenomenon known as twisted intramolecular charge transfer, which features a redshifted emission color and a decreased emission intensity with an increase in the polarity of the solvent.[6a,b,8c,d] In addition, the highly efficient combination of the aldehyde group and the activated methyl group provides a convenient method for the synthesis of TPE-TCF.

The thermal properties of TPE-TCF were investigated by TGA and differential scanning calorimetry (DSC) (see Figures S4 and S5, Supporting Information). The results show that TPE-TCF possesses high thermal stability with a decomposition temperature (T_d) of 358 °C. The theoretical calculation result of TPE-TCF is provided in the Supporting Information. As shown in Figure S6, Supporting Information, the TPE-TCF molecule mainly takes the HOMO and LUMO orbitals from the HOMO of TPE and LUMO of TCF units, respectively. This indicates that this molecule has pronounced D–A structure and the energy gap between the HOMO and LUMO orbitals is as narrow as 2.50 eV (see Table S1, Supporting Information). This was corroborated by the results of cyclic voltammetry (CV) measurements (Figure S7, Supporting Information).

According to our design rationale, integrating an electron donor (D, TPE moiety) and an acceptor (A, TCF moiety) into the same fluorophore should endow it with large dipole. Thus, its photophysical properties correlate to the polarity of the microenvironment. Solvatochromism is a representative of photophysical properties, in which the emission color of the molecule in solution depends on the solvent polarity.[12] We examined the effects of solvent polarity on the absorption and emission spectra of TPE-TCF and the results are displayed in Figure 1 A and B, respectively. The absorption spectra of TPE-TCF display next to no obvious changes upon changing the solvent polarity. From the apolar solvent cyclohexane to highly polar solvent acetonitrile, the absorption maxima only gave a small shift.

On the contrary, under the same measurement conditions as the absorption spectra, the recorded fluorescence (FL) spectra of TPE-TCF display evident polarity dependence (Figure 1 B). By changing the solvent from apolar cyclohexane to highly polar acetonitrile, the emission peak of TPE-TCF goes through an evident redshift of λ_{em} from 560 to 680 nm, corresponding to a redshift of 120 nm. Meanwhile, the emission intensity is distinctly decreased in ethanol and acetonitrile. The visual observations are displayed by the photographs in Figure 1 D. These behaviors clearly indicate a solvatochromic effect.

To describe the influences of solvent polarity on the emission behavior quantitatively, the Lippert–Mataga equation,[12a] which directly expresses the relationship between the Stokes shift and the solvent polarity parameter (Δf) was used. The

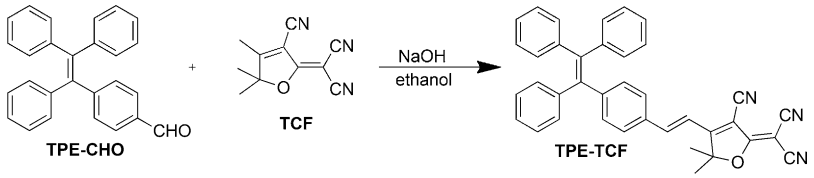

Scheme 1. Synthetic route to the target compound TPE-TCF.

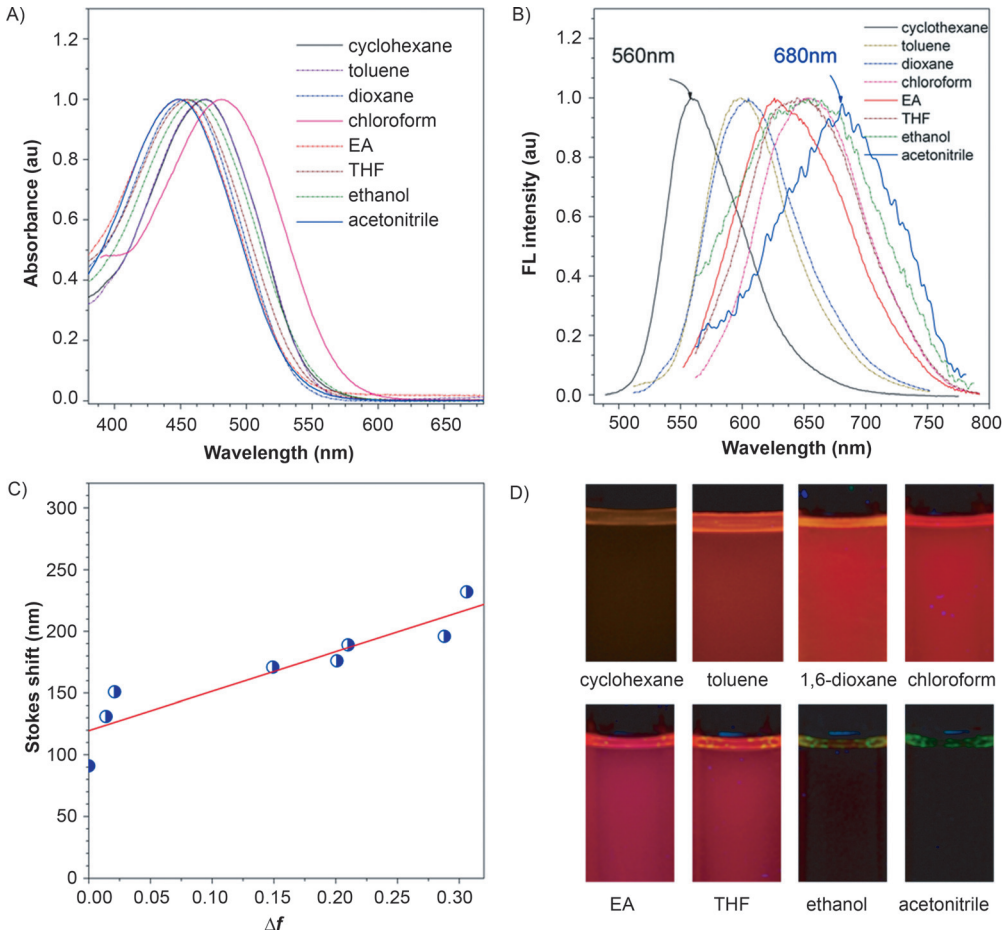

Figure 1. A) Normalized UV/Vis and B) fluorescence (FL) spectra of TPE-TCF in different solvents. The absorption maximum of each solution was chosen as its excitation wavelength. C) Plot of Stokes shift of TPE-TCF in each solvent versus Δf of the respective solvent. D) FL images of TPE-TCF solutions in different solvents taken under UV light. Concentration: 10 μM; solvents: cyclohexane, toluene, 1,4-dioxane, chloroform, ethyl acetate (EA), THF, ethanol, and acetonitrile.

normalized line is given in Figure 1C. On one hand, the Stokes shift is quite large: In acetonitrile, the shift is larger than 220 nm and in a less polar solvent, the Stokes shift is still over 150 nm. On the other hand, the data reveal an increasing tendency of the Stokes shifts with the increase of the solvent polarity and the slope of the fitted line is 319.7, which indicates a strong solvatochromic effect.

One of the photophysical properties that we are most interested in is whether the obtained TPE-TCF possess the inherent AIE properties from the TPE moiety or not. We checked the AIE character of TPE-TCF in THF/water mixtures, in which THF and water are the solvent and nonsolvent for TPE-TCF, respectively. It is a common procedure to verify AIE behavior in solvent/nonsolvent mixtures, because aggregates can gradually form when a suitable amount of nonsolvent is introduced into the solution. The obtained experimental results are shown in Figure 2. The absorption features of TPE-TCF show two trends with the variation of the water fraction (f_W, by volume%). As shown in Figure 2A, the absorption maximum shows a small redshift from 460 to 475 nm when f_W increases from 0 to 90%. Meanwhile, the absorbance remains unchanged when f_W is lower than 60%; but it decreases gradually when f_W is over 70%. The decrease of absorption intensity can be explained by the formation of aggregates in THF/water mixtures. The aggregates scatter the incident light and also reduce the number of the molecules available for light absorption.

In THF solution, TPE-TCF emits red fluorescence with an emission maximum at 630 nm (Figure 2B). This is quite satisfactory to us because we attempted to derive red-NIR-emitting fluorogens by using the strategy of introducing D and A moieties into the same fluorogen. The fluorescent quantum efficiency (Φ_F) of TPE-TCF in THF solution was measured to be 9.6%. When $f_w \leq 70\%$, the emission of the TPE-TCF in THF/water mixtures dramatically weakened and the emission spectrum redshifted (Figure 2B and C). When f_w was 70%, the fluorescence of the system was merely negligible and its Φ_F dropped to lower than 1%. The decrease of the fluorescence intensity can be ascribed to the twisted intramolecular charge-transfer process, which prescribes the low emission efficiency of a fluorogen with D–A structure in a highly polar solvent. The redshift of the emission spectrum is ascribed to the solvatochromic effect. When f_w is over 70%, the fluorescence of the system was intensified. The Φ_F rises to 8.9% and the peak emission wavelength shifts to 655 nm when f_w is up to 90%. The blue line in Figure 2C clearly shows this sharp transition. This observation can be attributed to the aggregate formation.

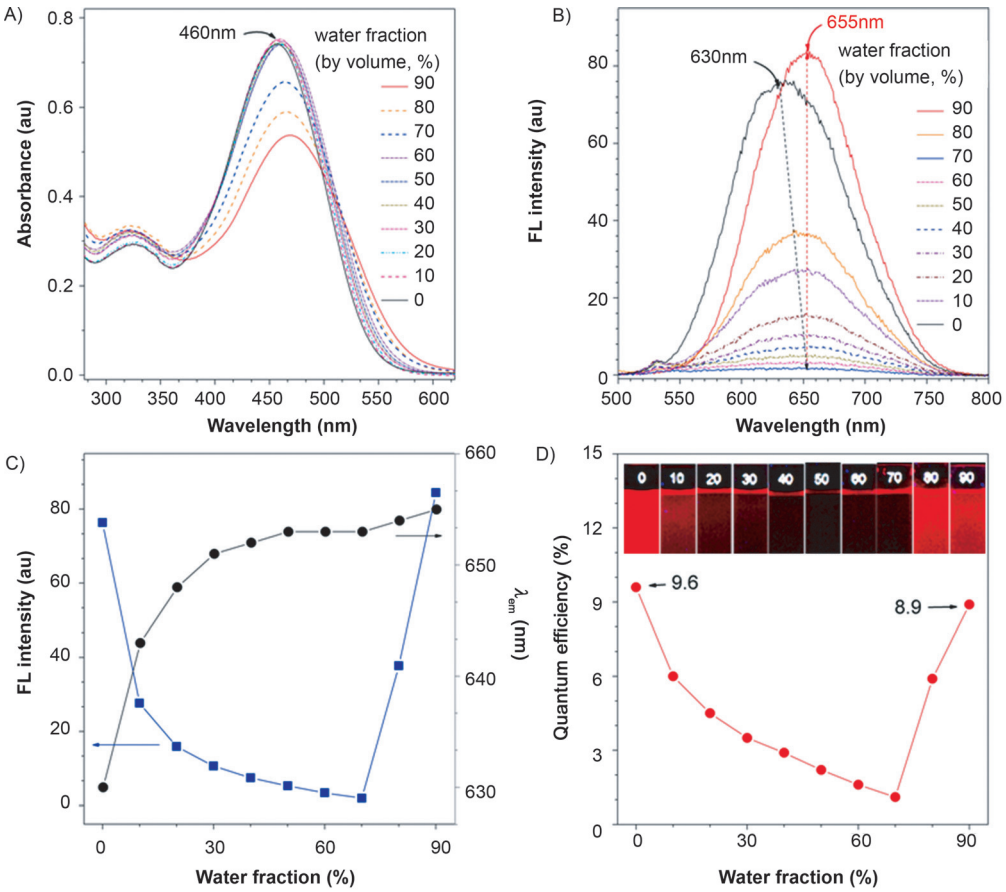

Figure 2. A) UV/Vis and B) fluorescence (FL) spectra of TPE-TCF in the THF/water mixtures with different water fractions (f_W). C) Plot of the changes of the peak FL intensity (blue) and peak wavelength (λ_{em}, black) of TPE-TCF with variation of f_W. D) Variation of Φ_F of TPE-TCF with f_W. Concentration: 10 μM. λ_{ex}: 460 nm. Inset of D): FL images for TPE-TCF in the THF/water mixtures taken under a UV lamp (λ_{ex}: 365 nm).

In solid film, the Φ_F of TPE-TCF is 24.8% and the emission peak appears at 670 nm (Figure S8, Supporting Information). For solid-state data of red to NIR emitting organic dyes, this efficiency is quite high and satisfactory for applications in cell staining and bioimaging.

Since it is insoluble in water, TPE-TCF cannot be directly employed as a fluorescent probe for cell staining. To solve this problem we fabricated nanoparticles (NPs) by a modified nanoprecipitation method[13] using 1,2-distearoylsn-glycero-3-phosphoethanolamine-*N*-[methoxy(poly-ethyleneglycol)-2000] (DSPE-PEG2000) modified with an HIV-1 tat protein (47-57) as the encapsulation matrix to yield NPs with good biocompatibilities (Figure 3).[14] TPE-TCF NPs represent TPE-TCF-based NPs that are formulated with polymers containing DSPE-PEG2000-tat in the polymer matrix. During the NP formation, the hydrophobic DSPE segments tend to be embedded into the hydrophobic core while the hydrophilic PEG2000-tat chains extend into the aqueous phase. Thus, TPE-TCF NPs have perfect water solubility, which enables the possibility for them to be used in bioimaging. Meanwhile, as the tat protein decorating the hydrophilic parts of the NPs is a widely used cell-penetrating peptide, it can greatly enhance the membrane penetrability of the NP-based materials.[15]

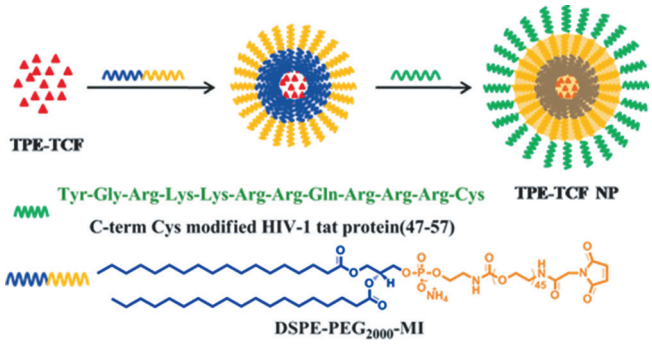

Figure 3. An illustration of the fabrication of NPs loaded with TPE-TCF.

Laser light scattering was used to measure the diameter of the synthesized TPE-TCF NPs (Figure 4A). The results suggest that the NP sample has a narrow size distribution and the average hydrodynamic diameter is around 99 nm. The morphology of the TPE-TCF NPs was studied by HR-TEM. The spherical shape of TPE-TCF NPs can be clearly distinguished from the black dots due to the high electron density of the TPE-TCF molecules. The particle size is approximately 95–100 nm (inset of Figure 4A and Figure S9, Supporting Information). The absorption and emission spectra of the TPE-TCF NPs in water are depicted in Figure 4B . Both of the absorption and emission

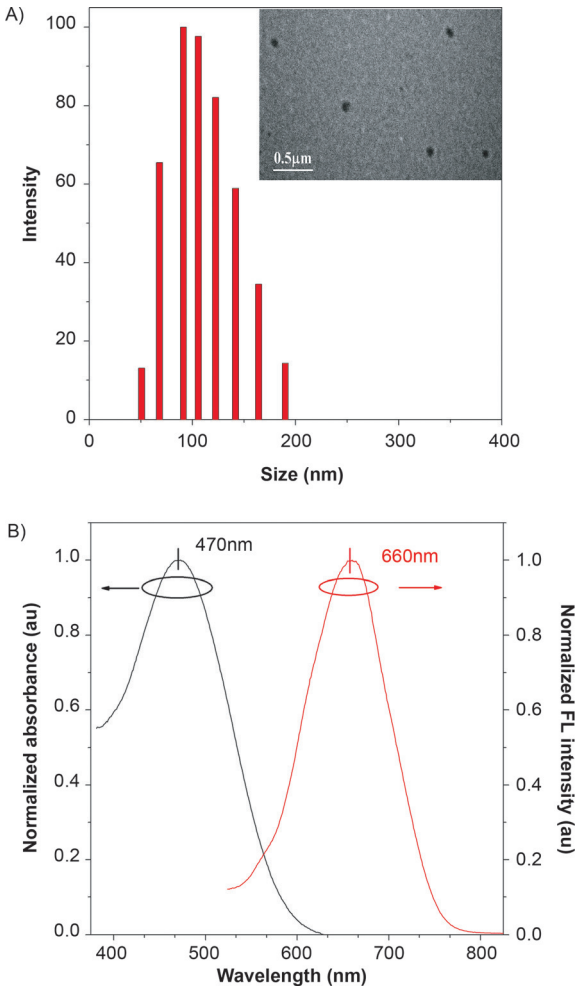

Figure 4. A) Particle-size distribution of TPE-TCF NPs in water studied via laser-light scattering. Inset: HR-TEM image of TPE-TCF NPs. B) Normalized UV and FL spectra of TPE-TCF NPs in water.

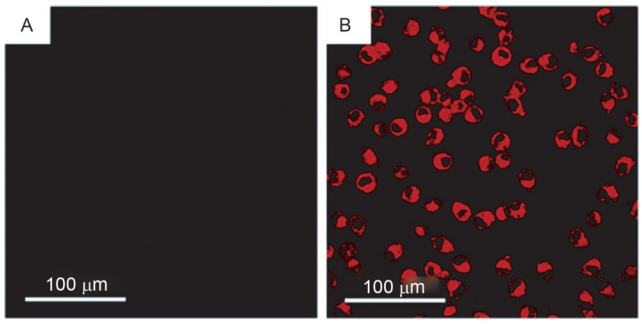

Figure 5. A) Confocal images of Hela cells incubated for 2 h at 37 °C without TPE-TCF NPs.B) Confocal images of the cells after incubation with TPE-TCF NPs for 2 h at 37 °C. The FL of TPE-TCF NPs was recorded at 600–700 nm with excitation at 405 nm. Concentration of TPE-TCF NPs: 2 μM.

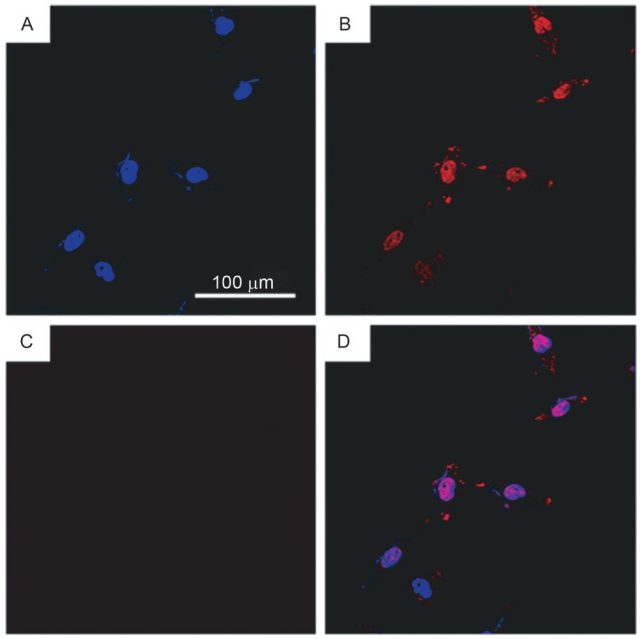

Figure 6. Confocal images of the cells after incubation in the presence of TPE-TCF NPs for 2 h at 37 °C recorded in the range of A) 450–490 nm and B) 600–700 nm at an excitation wavelength of 405 nm. C) Confocal image of Hela cells incubation for 2 h at 37 °C without TPE-TCF NPs. D) Overlapped image of A and B. Concentration of TPE-TCF NPs: 2 μM. The scale bar is the same for all images.

spectral shapes are similar to those of the nanoaggregates formed in the THF/water mixture with $f_w = 90\%$, with the absorption and emission maxima of the former redshifted to 470 and 660 nm, respectively. As shown in Figure 4B, due to the large Stokes shift, there is just a very small spectral overlap between the absorption and emission spectra of TPE-TCF NPs in water. In addition, Φ_F of TPE-TCF NPs is as high as 13.5%. These properties are beneficial to bioimaging.

The in vitro cytotoxicity of the obtained TPE-TCF NPs has been estimated against Hela cells using a Cell Counting Kit (CCK8) cell-viability assay. The histogram shown in Figure S10, Supporting Information, proves the low cytotoxicity of the AIE-active TPE-TCF NPs. Based on these results, the effect of the NPs' cell imaging has been studied by confocal laser scanning microscopy (CLSM). The details are provided in the Experimental Section. Figures 5 and 6 show the recorded images of Hela cells after incubation with TPE-TCF NP suspensions in a culture medium with and without 4,6-diamidino-2-phenylindole (DAPI) for 2 h, respectively. All of the images were taken upon excitation at 405 nm. As control experiments, we have done comparative cell stain experiments under the same conditions and it was found that without tat-protein modification, the DSPE-PEG2000-capsulated NPs could not enter into living cells, thus both the cell-staining and fluorescent imaging failed (Figure S11, Supporting Information) These results indicated that tat had been successfully modified onto the TPE-TCF NPs.

It is notable that no auto FL from the cell itself can be detected under the same experimental conditions (Figure 5A). After incubation with TPE-TCF NPs for 2 h, bright fluorescence can be observed in the cell cytoplasm, which indicates that the TPE-TCF NPs can go through the cell membrane smoothly. Meanwhile, no FL can be detected in the cell nucleus, which means that the NPs could not pass the nuclear membrane (Figure 5B). The photograph also shows that the fluorescence is quite bright and it covers almost all the cytoplasm part of

the cell. This observation demonstrates that TPE-TCF NPs evenly distribute themselves within the cytoplasm.

To confirm that TPE-TCF NPs have not entered into the cell nucleus, DAPI, a typical fluorescent dye for nuclear staining, was used as a calibration to stain the cell nucleus. As shown by the FL images in Figure 6A and B, bright blue (FL from DAPI received at 450–490 nm) and red fluorescence (FL from TPE-TCF NPs received at 600–700 nm) could be recorded in the cell nucleus and partly observed in the cell cytoplasm when TPE-TCF NPs and DAPI molecules were concomitantly used in the cell staining process. Figure 6D displays the merged images of Figure 6A and B, which indicates very good overlapping. This result seems to be incompatible with that observed in Figure 5. In fact, the treatment procedures in the two cases are different. To let DAPI molecules penetrate into the nucleus of the living cells, triton has to be added into the incubation media to enlarge the size of the nuclear pore. Meanwhile, on the surface of the NPs, each tat has six Arg residues. These plentiful Arg residues make the TPE-TCF NPs positively charged in aqueous media, which may be advantageous to the attractive interaction between TPE-TCF NPs and negatively charged cell nucleus. However, without DAPI concomitantly existing in the cell staining process, the control experiment suggested that overlapping of the fluorescent and optical images for the nucleus of the living cells is found only in rare cases (Figure S12, Supporting Information). Comparing the images in Figure 6 with those demonstrated in Figure 5 and Figure S12, in the presence of DAPI and triton, it can be seen that DAPI plays a helpful role for the interaction between TPE-TCF NPs and the cell nucleus. This interesting research topic is undergoing further investigation.

Conclusion

In summary, an AIE-active fluorescent dye, TPE-TCF, has been prepared. Its emission spectrum covers the red and partial NIR region and the emission maximum shifts from 630 to 670 nm from when in a THF solution to the solid film. The quantum efficiency of the solid film is as high as 24.8%. In comparison with previously reported AIE-active red-NIR emission dyes, the synthetic route to TPE-TCF is short, containing only two simple steps. Thus, the total yield is as high as 72%. TPE-TCF exhibits an intramolecular charge-transfer from the TPE core to the TCF unit, which leads to a pronounced solvatochromic effect and a 120 nm redshifted emission from apolar to highly polar solvents has been recorded. Taking the advantage of the red-NIR emission and high quantum yield, TPE-TCF was tested in cell-imaging studies. By loading the dye molecules into the micelles built from the amphiphilic copolymer DSPE-PEG2000-tat, TPE-TCF NPs have been fabricated. The NPs are spherical in shape with a diameter of about 100 nm and a narrow particle-size distribution. They are red fluorescent with an emission peak at around 660 nm and a Stokes shift as large as 190 nm. After incubation with Hela cells for 2 h, the confocal images show that TPE-TCF NPs are evenly internalized in the cell cytoplasm. Upon co-incubation with DAPI (an organic dye that is typically used for staining cell nuclei), TPE-TCF NPs demonstrated a trend to concentrate in the nuclear region. Reasonably, we can expect that this can be applied in more bioimaging situations when the NPs are decorated with different modifiers besides the tat peptide.

Experimental Section

Materials

4-Bromobenzophonene and diphenylmethane were purchased from Alfa Aesar. *n*BuLi, *N*-formylpiperdine, malononitrile, magnesium ethoxide, and 3-hydroxy-3-methylbutan-2-one were purchased from J&K. 1,2-Distearoyl-sn-glycero-3-phosphoethanolamine-*N*-[maleimide(poly- ethylene glycol)-2000] (DSPE-PEG2000-Maleimide) was purchased from Avanti, HIV-1 tat protein(47–57)-Cys (Tyr-Gly-Arg-Lys-Lys-Arg-Arg-Gln-Arg-Arg-Arg-Cys), DAPI and Cell-culture products were purchased from Invitrogen Gibco. Other reagents including *p*-toluene-sulfonic acid (TsOH), magnesium sulfate, ammonium chloride, toluene, ethanol, ethyl acetate (EA), petroleum ether (PE), and dichloromethane (DCM) were purchased from Sinopharm Chemical Reagent Co., Ltd. THF was distilled under normal pressure from sodium benzophenone ketyl under nitrogen immediately prior to use.

Instrumentation

^{1}H and ^{13}C NMR spectra were measured on a Mercury plus 400 MHz NMR spectrometer in $CDCl_3$ with tetramethylsilane (TMS; $\delta = 0$ ppm) as the internal standard. Elemental analysis was performed on a ThermoFinnigan Flash EA1112 apparatus. UV absorption spectra were taken on a Varian CARY 100 Biospectrophotometer. PL spectra were recorded on a spectrofluorophotometer (RF-5301PC, SHIMADZU, Japan). SEM images were taken on a JSM-5510 (JEOL, Japan) scanning electron microscope. Fluorescent images were taken with a Zeiss Axiovert 200 inverted microscope equipped with a 100× oil immersion objective with a numerical aperture of 1.4 and an Ebq 100 Isolated electronic ballast for mercury vapour compressed-arc lamps. TGA spectra were recorded on a DSCQ 1000 (TA, USA) calorimeter. The morphology of the NPs was studied by using a HR-TEM (JEM-2010F, JEOL, Japan). The average particle size and size distribution of the NPs were determined by laser light scattering with particle-size analyzer (90 Plus, Brookhaven Instruments Co. USA) at a fixed angle of 90° at room temperature. The cell images were taken on an upright Olympus laser scanning confocal microscope (FV1000).

Synthesis of 2-(3-cyano-4,5,5-trimethylfuran-2(5*H*)ylidene)-malononitrile (TCF)

Malononitrile (5.9 g, 90 mmol) and magnesium ethoxide (3.8 g, 34 mmol) were added into a 100 mL two-necked round-bottomed flask under nitrogen. 3-Hydroxy-3- methylbutan-2-one (3.2 mL, 30 mmol) and then 30 mL of ethanol were injected into the flask and the temperature was increased to 60 °C. After stirring at 60 °C for 8 h, the mixture was cooled to room temperature and then evaporated. After that, 100 mL of DCM was added into the system and the mixture was filtered. The filtrate was washed with brine and dried over anhydrous magnesium sulfate. After filtration and solvent evaporation, the residue was purified by silica gel column chromatography, using DCM as the eluent and was then recrystallized from ethanol. TCF (8.2 g) was obtained as a yellow crystal in 68.0% yield. ^{1}H NMR (400 MHz, $CDCl_3$): $\delta = 2.37$ (s, 3H, CH_3),

1.63 ppm (s, 6H, CH_3); ^{13}C NMR (100 MHz, $CDCl_3$): $\delta = 182.69$, 175.25, 111.06, 110.45, 109.00, 104.78, 99.83, 24.38, 14.24 ppm.

Synthesis of 2-(3-cyano-5,5-dimethyl-4-(4-(1,2,2-triphenylvinyl)styryl)furan-2(5*H*)ylidene)malononitrile (TPE-TCF)

4-(1,2,2-Triphenylvinyl)benzaldehyde (TPE-CHO) was synthesized according to our previously published paper.[10] A mixture of TPE-CHO (0.74 g, 2.0 mmol), TCF (0.50 g, 2.5 mmol), and NaOH (4.2 mg) were added into a 100 mL two-necked round-bottomed flask. The flask was evacuated under vacuum and flushed with dry nitrogen three times. Ethanol (25 mL) was injected into the flask and the mixture was refluxed overnight. After the reaction had been completed, the mixture was extracted with DCM. The organic layer was washed with brine and dried over anhydrous magnesium sulfate. After filtration and solvent evaporation, the residue was purified by silica gel column chromatography, using PE/DCM/EA (200:100:1 by volume) as the eluent. TPE-TCF (0.78 g) was obtained as a bright-red solid in 72% yield. ^1H NMR (400 MHz, $CDCl_3$): $\delta = 7.56$–7.52 (d, 1H, CH), 7.39–7.36 (d, 2H, Ar H), 7.16–7.00 (m, 17H, Ar H), 6.92–6.97 (d, 1H; CH), 1.77 ppm (s, 4H, CH_3); ^{13}C NMR (100 MHz, $CDCl_3$): $\delta = 175.55$, 174.10, 149.61, 147.31, 143.64, 143.32, 143.21, 143.08, 139.85, 132.77, 131.98, 131.57, 131.48, 128.79, 128.24, 128.22, 127.99, 127.43, 127.22, 114.63, 111.92, 111.15, 110.47, 99.80, 97.83, 26.74 ppm; HRMS (MALDI-TOF) *m/z*: $[M]^+$; elemental analysis calcd (%) for $C_{38}H_{27}N_3O$: 541.2154; found: 541.2150 (see Figure S3, Supporting Information); elemental analysis calcd (%) for $C_{38}H_{27}N_3O$: C 84.26, H 5.02, N 7.76; found: C 84.02, H 4.90, N 7.71.

Synthesis of TPE-TCF NPs

A THF solution (1 mL) containing 1 mg of TPE-TCF and 2 mg of DSPE-PEG2000-Maleimide was added into 9 mL of water drop by drop at room temperature. This was followed by sonicating the mixture for 60 s at 12 W output by using a microtip probe sonicator (XL2000, Misonix Incorporated, NY). The obtained solution was filtered over a 0.22 μm syringe-driven filter and the filtrate was stirred at room temperature for 12 h to evaporate the THF. Then, 2 mL of the emulsion was added into 8 mL of water that contained 0.7 mg of Tat-cys. The mixture was stirred at room temperature for another 12 h and then dialyzed by a 3500 Mw dialysis tube for 2 days to get the products.

Cell culture and imaging

HeLa cells (human cervical carcinoma cell lines) were cultivated in Dulbecco minimum essential media (DMEM) with 10% fetal bovine serum (FBS), 1% penicillin, and 1% amphotericin B. One day before the treatment, the cells were seeded in 35 mm cultivation dishes at a confluence of 70–80%. For cell imaging, a 200 μL aqueous solution of the TPE-TCF nanoparticles was added into the cell plate with HeLa cells and incubated for 2 h. After that, the cells were gently washed thrice with phosphate-buffered saline (PBS, pH 7.4, 10 mM) and fixed by paraformaldehyde for 15 min under 4 °C. Then, triton was added in to the cell plate and it was kept at 4 °C for 15 min to increase the permeability of the cell membrane. Lastly, DAPI was added and the cell plate was kept in a dark place for 10 min at room temperature. Then the cells were imaged with FV1000.

Viability analysis

Hela cells were kept in Dulbecco's modified eagle's medium (DMEM; Gibco) supplemented with 10% fetal bovine serum (FBS; Hyclone) at 37 °C and 5% CO_2. The effect of TPE-TCF NPs on cell viability was determined using a WST-8 cell counting kit (CCK-8, Dojindo Laboratories in Japan). Briefly, cells were seeded in 96-well plates at 2000 cell/per well. After incubation for 24 h, cells were treated with TPE-TCF NPs and incubated for another 24 h. Lastly, the cells were added to the CCK8 reagent with a measured optical density (OD) of 450 nm to evaluate cell viability.

Acknowledgements

This work was financially supported by the key project of the Ministry of Science and Technology of China (2013CB834704), the National Science Foundation of China (51573158, 51273175), the Research Grants Council of Hong Kong (16301614, N_HKUST604/14, N_HKUST620/11). J. Z. Sun thanks financial support from Zhejiang Innovative Research Team Program (2013TD02). A. Qin and B. Z. Tang thank support from Guangdong Innovative Research Team Program (201101C0105067115).

Keywords: aggregation-induced emission · cell-imaging · red-NIR fluorescence · solvatochromism · Stokes shift

[1] a) Y. Xu, Q. Liu, X. Li, C. Wesdemiotisa, Y. Pang, *Chem. Commun.* **2012**, *48*, 11313 – 11315; b) M. Li, X. Wu, Y. Wang, Y. Li, W. Zhu, T. D. James, *Chem. Commun.* **2014**, *50*, 1751 – 1753; c) Y. Qu, J. Hua, H. Tian, *Org. Lett.* **2010**, *12*, 3320 – 3323; d) S. Kim, H. E. Pudavar, A. Bonoiu, P. N. Prasad, *Adv. Mater.* **2007**, *19*, 3791 – 3795; e) J. Gao, B. Xua, *Nano Today* **2009**, *4*, 37 – 51; f) J. Wiedenmann, F. Oswald, G. U. Nienhaus, *IUBMB Life* **2009**, *61*, 1029 – 1042.

[2] W. Zhu, X. Huang, Z. Guo, X. Wu, H. Yu, H. Tian, *Chem. Commun.* **2012**, *48*, 1784 – 1786.

[3] X. Li, S. Qian, Q. He, B. Yang, J. Li, Y. Hu, *Org. Biomol. Chem.* **2010**, *8*, 3627 – 3630.

[4] B. Tang, Y. Xing, P. Li, N. Zhang, F. Yu, G. Yang, *J. Am. Chem. Soc.* **2007**, *129*, 11666 – 11667.

[5] S. Sreejith, K. P. Divya, A. Ajayaghosh, *Angew. Chem. Int. Ed.* **2008**, *47*, 7883 – 7887; *Angew. Chem.* **2008**, *120*, 8001 – 8005.

[6] a) J. Mei, Y. Hong, J. W. Y. Lam, A. Qin, Y. Tang, B. Z. Tang, *Adv. Mater.* **2014**, *26*, 5429 – 5479; b) Y. Hong, J. W. Y. Lam, B. Z. Tang, *Chem. Soc. Rev.* **2011**, *40*, 5361 – 5388; c) Z. J. Zhao, J. W. Y. Lam, B. Z. Tang, *J. Mater. Chem.* **2012**, *22*, 23726 – 23740; d) M. Chen, L. Li, H. Nie, J. Tong, L, Yan, B. Xu, J. Z. Sun, W, Tian, Z. Zhao, A. Qin, B. Z. Tang, *Chem. Sci.* **2015**, *6*, 1932 – 1937.

[7] J. D. Luo, Z. L. Xie, J. W. Y. Lam, L. Cheng, H. Y. Chen, C. F. Qiu, H. S. Kwok, X. W. Zhan, Y. Q. Liu, D. B. Zhu, B. Z. Tang, *Chem. Commun.* **2001**, 1740 – 1741.

[8] a) Q. Zhao, K. Li, S. Chen, A. Qin, D. Ding, S. Zhang, Y. Liu, B. Liu, J. Z. Sun, B. Z. Tang, *J. Mater. Chem.* **2012**, *22*, 15128 – 15135; b) W. Qin, D. Ding, J. Liu, W. Z. Yuan, Y. Hu, B. Liu, B. Z. Tang, *Adv. Funct. Mater.* **2012**, *22*, 771 – 779; c) W. Qin, K. Li, G. Feng, M. Li, Z. Yang, B. Liu, B. Z. Tang, *Adv. Funct. Mater.* **2014**, *24*, 635 – 643; d) S. Chen, Y. Hong, Y. Liu, J. Liu, C. W. T. Leung, M. Li, R. T. K. Kwok, E. Zhao, J. W. Y. Lam, Y. Yu, B. Z. Tang, *J. Am. Chem. Soc.* **2013**, *135*, 4926 – 4929.

[9] R. R. Hu, E. Lager, A. Aguilar-Aguilar, J. Z. Liu, J. W. Y. Lam, H. H. Y. Sung, I. D. Williams, Y. C. Zhong, K. S. Wong, E. Pena-Cabrera, B. Z. Tang, *J. Phys. Chem. C* **2009**, *113*, 15845 – 15853.

[10] a) X. Chen, X. Y. Shen, E. Guan, Y. Liu, A. Qin, J. Z. Sun, B. Z. Tang, *Chem. Commun.* **2013**, *49*, 1503 – 1505; b) J. Mei, J. Tong, J. Wang, A. Qin, J. Z. Sun, B. Z. Tang, *J. Mater. Chem.* **2012**, *22*, 17063 – 17070.

[11] a) Q. Zhao, S. Zhang, Y. Liu, J. Mei, S. Chen, P. Lu, A. Qin, Y. Ma, J. Z. Sun, B. Z. Tang, *J. Mater. Chem.* **2012**, *22*, 7387 – 7394; b) X. Y. Shen, Y. J. Wang, E. Zhao, W. Z. Yuan, Y. Liu, P. Lu, A. Qin, Y. Ma, J. Z. Sun, B. Z. Tang, *J. Phys. Chem. C* **2013**, *117*, 7334 – 7347; c) Z. Zhao, S. Chen, J. W. Y. Lam, P. Lu, Y. Zhong, K. S. Wong, H. S. Kwok, B. Z. Tang, *Chem. Commun.*

2010, *46*, 2221 – 2223; d) Z. Zhao, P. Lu, J. W. Y. Lam, Z. Wang, C. Y. K. Chan, H. H. Y. Sung, I. D. Williams, Y. Ma, B. Z. Tang, *Chem. Sci.* **2011**, *2*, 672 – 675.

[12] a) C. Reichardt, *Chem. Rev.* **1994**, *94*, 2319 – 2358; b) Y. Zhang, D. Li, Y. Lia, J. Yu, *Chem. Sci.* **2014**, *5*, 2710 – 2716; c) M. Sun, S. Wang, Q. Yang, X. Fei, Y. Li, Y. Li, *RSC Adv.* **2014**, *4*, 8295 – 8299; d) M. K. Bera, C. Chakraborty, P. K. Singh, C. Sahu, K. Sen, S. Maji, A. K. Dasc, S. Malik, *J. Mater. Chem. B* **2014**, *2*, 4733 – 4739.

[13] a) C. Prashant, M. Dipak, C. T. Yang, K. H. Chuang, D. Jun, S. S. Feng, *Biomaterials* **2010**, *31*, 5588 – 5597; b) K. Li, Y. Jiang, D. Ding, X. Zhang, Y. Liu, J. Hua, S.-S. Feng, B. Liu, *Chem. Commun.* **2011**, *47*, 7323 – 7325.

[14] M. Lindgren, M. Hällbrink, A. Prochiantz, Ü. Langel, *Trends Pharmacol. Sci.* **2000**, *21*, 99 – 103.

[15] H. Brooks, B. Lebleu, E. Vive's, *Adv. Drug Delivery Rev.* **2005**, *57*, 559 – 577.

Received: January 12, 2016
Published online on June 6, 2016